Steering Behavior of an Articulated Amphibious All-Terrain Tracked Vehicle

Steering behavior of an Articulated Amphibious All-Terrain Tracked Vehicle

Author, co-author (Do NOT enter this information. It will be pulled from participant tab in MyTechZone)

Affiliation (Do NOT enter this information. It will be pulled from participant tab in MyTechZone)

Abstract

This paper presents a study related to an Articulated Amphibious All-Terrain Tracked Vehicle (ATV) characterized by a modular architecture. The ATV is composed by two modules: the first one hosts mainly the vehicle engine and powertrain components, meanwhile the second one can be used for goods transportation, personnel carrier, crane and so on. The engine torque is transmitted to the front axle sprocket wheel of each module and finally distributed on the ground through a track mechanism. The two modules are connected through a multiaxial joint designed to guarantee four relative degrees of freedom. To steer the ATV, an Electro Hydraulic Power System (EHPS) is adopted, thus letting the vehicle steerable on any kind of terrain without a differential tracks speed. The paper aims to analyze the steady-state lateral behavior of the ATV on a flat road, through a non-linear mathematical vehicle model built in Matlab/Simulink environment. The model describes the vehicle main planar motion and the interaction between the two modules through the application of a hydraulic steering torque. The model simulates steady-state handling maneuvers in Matlab/Simulink. Two scenarios are considered: one with the application of an open-loop hydraulic steering torque without any vehicle feedback; the second one with a closed-loop steering torque actuation based on the relative angle between the two modules (hitch angle). Finally, the influence of the ATV longitudinal speed on vehicle lateral characteristics is also presented.

Introduction

Tracked vehicles have been always of engineering interest due to their key role in off-road or all-terrain applications [1-3]. Most tracked vehicles adopt what is normally called skid steering whereby the tracks on either side of the vehicle are driven at different speeds [4-7]. This is usually a very common solution for military applications where double differential mechanisms are designed to produce the speed difference between the tracks [8-9]. The main drawback of the skid-steering solution is that it limits the vehicle maneuverability in presence of high traction request conditions. High tractive requirements usually lead to limit steer angles because of high longitudinal slips. One of the methods of overcoming these problems is to design the vehicle with articulated frame steering [10]. This allows high steering angles to be achieved. With an articulation joint connecting the two separate sections, articulated steer vehicles can be steered by two hydraulic cylinders. This results in the widely use of articulated steer vehicles in agricultural, construction, forestry, and mining sectors. For these and other economic reasons, this type of vehicle layout has become commonplace. The hydraulic steering system plays a critical role in keeping the directional stability and tracking the steer-handling capability of the vehicle [11-12]. Many activities have been carried out to model and analyze the behavior of the hydraulic steering system [13].

Apart from the steering mechanism of the vehicle, the kinematics and dynamics of the hydraulic articulated frame steering system play a critical role in retaining directional stability of the vehicle, since articulated steer vehicles are inherently directionally unstable and exhibit a jack-knife tendency about the pivot, particularly at higher speeds. These vehicles also operate on paved roads at relatively higher speeds and thus, pose difficult handling and directional performance requirements.

In this framework, the study presented in this paper aims to provide further insights related to the handling characteristics of this vehicles. The analysis is carried based on an Articulated Amphibious All-Terrain Tracked Vehicle (ATV) characterized by a modular architecture whose behavior is simulated by a non-linear mathematical model of 8 degrees of freedom: longitudinal, lateral and yaw motion of the front module, yaw motion of the rear module and rotational motions of the 4 sprocket wheels, two for each module. The distributed contact between tracks and terrain is modelled with a discrete number of contact patches equal to the number of road wheels, as assumed also by [4-5, 14-16]. The objectives of the paper are:

- Understand the effect of controlling the steering torque in open-loop and closed-loop conditions
- Provide handling characteristics able to describe the overall steady-state behavior of the ATV
- Evaluate the vehicle longitudinal speed influence on handling characteristics

The paper is divided into three main sections: the first one is related to the mechanical description of the ATV vehicle considered; in the following section, the non-linear model equations are introduced; Simulation results during steady-state maneuvers are shown and commented within the third section. Finally, some conclusions are drawn in the last section.

ATV Architecture Description

The ATV, focus of the present research activity, is shown in Fig.1. The vehicle is composed by two modules: the front module hosts the

internal combustion engine with a six-speed automatic transmission and a transfer box used to extend its driving range with two auxiliary gear ratios; The second module has the main purpose of goods and personnel transportation. Each module weight can be supported by 4 or 5 couples of road wheels, depending on load conditions.

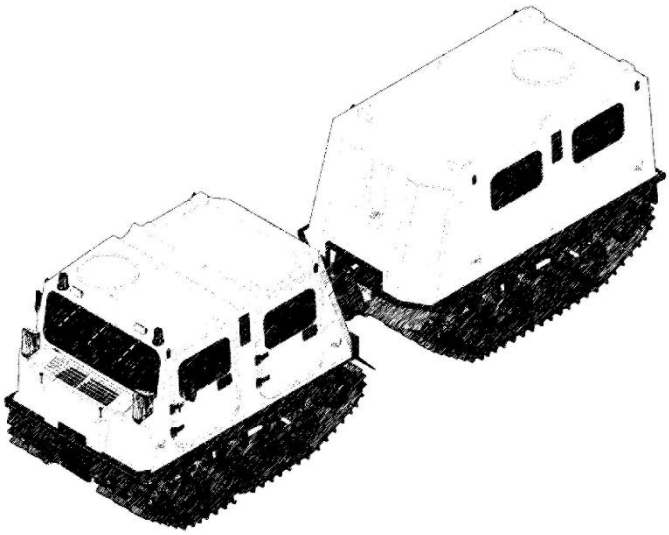

Figure 1. Picture of Amphibious All-Terrain Vehicle from ARIS-spa.

Each road wheel is connected to the hull through appropriate torsional bars that, together with specific bushings, constitute the elastic-damping components of ATV. All road wheels are moved by four sprocket wheels (one for each module side) through a track mechanism. The engine torque is equally distributed between the two modules and between the two sprocket wheels through open differentials. The ATV steering is entrusted to a specific mechanical connection joint which consists of 5 hinges thus allowing 4 relative degrees between the two modules, as shown in Fig. 2. The EHPS is composed by a hydraulic proportional valve able to control the flow rate towards two hydraulic cylinders, thus providing a steering torque C_s, with same amplitude but different sign, to each module.

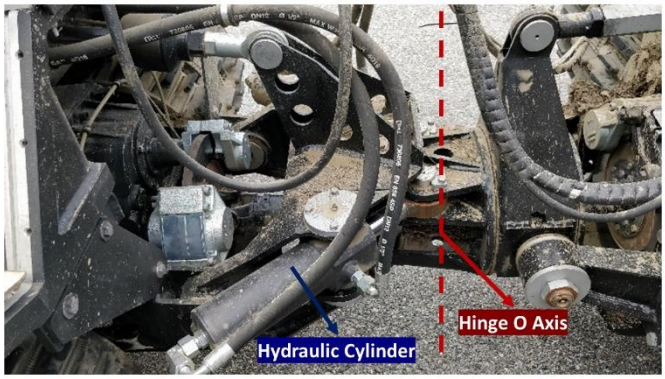

Figure 2. Details of multiaxial joint between the two modules.

Non-Linear Mathematical Model

The mathematical model has 8 degrees of freedom (8-DOF): longitudinal, lateral and yaw motion of the front module, yaw motion of the rear module and rotational motion of the 4 sprocket wheels.

Main assumptions for modelling the vehicle planar motion are:

- Modules as considered as rigid bodies, with masses m_1 and m_2 and moments of inertia around z-axis I_{G1} and I_{G2}
- 8 road wheels are considered for each module, 4 for right and 4 for left sides
- Continuous track-terrain contact is discretized in a finite number of contact patches equal to the number of road wheels. Contact patch forces are modelled as smoothed friction functions depending on the longitudinal slip and slip angle of the tracks
- Longitudinal and lateral forces interaction is modelled using look-up tables
- The static vertical load and lateral load transfers are only applied in the contact points of road wheels
- Rigid transmission components, i.e., no compliance effects are considered, and no gear backlash in the transmission
- Load transfers due to longitudinal acceleration is neglected since the paper focus is on cornering behaviors
- Rigid road, the effect of sinkage is neglected
- Adhesion on the track-terrain interface is neglected
- Terrain inclination is neglected

Bodies Dynamics

Fig. 3 shows the ATV top view where three reference systems are introduced: the absolute reference coordinate system R_O (X, Y, Z) fixed to the ground, a moving reference coordinate system R_1 (x_1, y_1, z_1) centered on the front module's center of gravity G_1 and a moving reference coordinate system R_2 (x_2, y_2, z_2) centered on the rear module's center of gravity G_2.

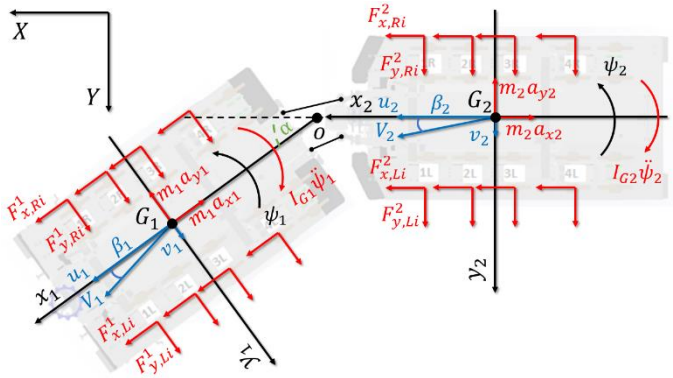

Figure 3. Free body diagram of ATV (top view).

The velocity of front and rear modules center of gravity are described by vectors V_1 and V_2 respectively, composed by longitudinal (u_1 and u_2) and lateral (v_1 and v_2) components expressed in their respective reference systems R_1 and R_2. The angles between V_1 and V_2 with respect to longitudinal direction are identified by sideslip angles β_1 and β_2 respectively. The longitudinal direction of each module is defined by their yaw angles ψ_1 and ψ_2 with respect the global reference frame X-axis. The difference $\alpha = \psi_1 - \psi_2$ represents the hitch angle or relative angle between the two modules.

The continuous track-terrain contact force is described by an equivalent system composed by four contact forces, one for each road wheel. Each contact force is expressed by two components, $F^k{}_{xj,i}$ and $F^k{}_{yj,i}$, where $k = 1, 2$ refers to the front and rear modules, $j = L, R$ to left and right track side and $i = 1, .., N = 4$ to each track-terrain contact point.

The ATV longitudinal and lateral dynamics balance equations are described by:

$$m_1 a_{x1} = \sum_{i=1}^{N} F_{x,Li}^1 + \sum_{i=1}^{N} F_{x,Ri}^1 + \\ + \left[\sum_{i=1}^{N} F_{x,Li}^2 + \sum_{i=1}^{N} F_{x,Ri}^2 - m_2 a_{x2}\right]\cos\alpha + \\ + \left[\sum_{i=1}^{N} F_{y,Li}^2 + \sum_{i=1}^{N} F_{y,Ri}^2 - m_2 a_{y2}\right]\sin\alpha \quad (1)$$

$$m_1 a_{y1} = \sum_{i=1}^{N} F_{y,Li}^1 + \sum_{i=1}^{N} F_{y,Ri}^1 + \\ - \left[\sum_{i=1}^{N} F_{x,Li}^2 + \sum_{i=1}^{N} F_{x,Ri}^2 - m_2 a_{x2}\right]\sin\alpha + \\ + \left[\sum_{i=1}^{N} F_{y,Li}^2 + \sum_{i=1}^{N} F_{y,Ri}^2 - m_2 a_{y2}\right]\cos\alpha \quad (2)$$

where a_{x1}, a_{y1} are the front module longitudinal and lateral acceleration components expressed with respect to R_1 and a_{x2}, a_{y2} are the rear module longitudinal and lateral acceleration components expressed with respect to R_2.

The two modules yaw dynamics balance equations, with respect their relative center of gravity, are expressed by:

$$I_{G1}\ddot{\psi}_1 = \sum_{i=1}^{N} \underbrace{\left[\frac{(F_{x,Ri}^1 - F_{x,Li}^1)T}{2} + (F_{y,Li}^1 + F_{y,Ri}^1)d_i^1\right]}_{M_z^1} + \\ + C_s - m_1 a_{y1} x_{G1} - c_O\dot{\alpha} \quad (3)$$

$$I_{G2}\ddot{\psi}_2 = \sum_{i=1}^{N} \underbrace{\left[\frac{(F_{x,Ri}^2 - F_{x,Li}^2)T}{2} - (F_{y,Li}^2 + F_{y,Ri}^2)d_i^2\right]}_{M_z^2} + \\ - C_s + m_2 a_{y2} x_{G2} + c_O\dot{\alpha} \quad (4)$$

where $\ddot{\psi}_1$ and $\ddot{\psi}_2$ are the front and rear modules yaw acceleration respectively; d_i^1 and d_i^2 are the longitudinal distances of i_{th} road wheel from the joint O respectively; x_{G1} and x_{G2} are the distances of G_1 and G_2 from the joint O respectively; T is the track width; c_O is the joint O damping coefficient which includes the combined damping contributions from the joint bushing and the hydraulic oil resistance. M_z^1 and M_z^2 are the yaw moments of front and rear modules track-terrain contact forces respectively. M_z^k is supposed to overcome lateral shear resistance while lateral bulldozing resistance is neglected. The amplitude of this turning moment accounts for the non-uniform pressure distribution between tracks and terrain due to the lateral load transfer.

The hinge O constrains the relative motion of rear module with respect to the front one:

$$\begin{cases} a_{x2} = (a_{x1} + \dot{\psi}_1^2 x_{G1})\cos\alpha - (a_{y1} - \ddot{\psi}_1 x_{G1})\sin\alpha + \dot{\psi}_2^2 x_{G2} \\ a_{y2} = (a_{x1} + \dot{\psi}_1^2 x_{G1})\sin\alpha + (a_{y1} - \ddot{\psi}_1 x_{G1})\cos\alpha - \ddot{\psi}_2 x_{G2} \end{cases} \quad (5)$$

where $\dot{\psi}_1$ and $\dot{\psi}_2$ are front and rear module yaw rates.

Eq. (5) is used to simplify a_{x2} and a_{y2} from Equations (1)-(4) thus obtaining four second order differential equations with only variable related to longitudinal, lateral and yaw motion of first module and the yaw motion of the rear module. Linear accelerations are related to vehicle speed components by:

$$\begin{cases} a_{x1} = \dot{u}_1 - v_1\dot{\psi}_1 \\ a_{y1} = \dot{v}_1 + u_1\dot{\psi}_1 \\ a_{x2} = \dot{u}_2 - v_2\dot{\psi}_2 \\ a_{y2} = \dot{v}_2 + u_2\dot{\psi}_2 \end{cases} \quad (6)$$

Linear (u_k , v_k) and angular speeds ($\dot{\psi}_k$) are calculated by integrating their correspondent derivatives $\dot{u}_k$, $\dot{v}_k$ and $\ddot{\psi}_k$ from Equation 6. ATV velocity vectors are characterized by their amplitude and sideslip angle:

$$\begin{cases} V_1 = \sqrt{u_1^2 + v_1^2} \\ V_2 = \sqrt{u_2^2 + v_2^2} \end{cases} \quad (7)$$

$$\begin{cases} \beta_1 = \operatorname{atan}\dfrac{v_1}{u_1} \\ \beta_2 = \operatorname{atan}\dfrac{v_2}{u_2} \end{cases} \quad (8)$$

Each module absolute position (X_1, Y_1) and (X_2, Y_2) with respect to R_O is finally obtained by:

$$X_1 = \int (u_1\cos\psi_1 - v_1\sin\psi_1) \\ Y_1 = \int (v_1\cos\psi_1 + u_1\sin\psi_1) \\ X_2 = \int (u_2\cos\psi_2 - v_2\sin\psi_2) \\ Y_2 = \int (v_2\cos\psi_2 + u_2\sin\psi_2) \quad (9)$$

Track-Terrain contact forces

Since ground loading is concentrated under the road wheels, the continuous track-terrain contact force distribution is modelled as an equivalent lumped system in order to obtain the same total longitudinal, lateral forces and yaw moments, as assumed also by [4,5,14]. The forces are then discretized into several contact patches equal to the number of road wheels through a hyperbolic tangent function:

$$F_{xj,i}^{k} = k_{\beta}\mu F_{zj,i}^{k}\tanh\frac{3\sigma_{j,i}^{k}}{\sigma_{max}}$$
$$F_{yj,i}^{k} = k_{\sigma}\mu F_{zj,i}^{k}\tanh\frac{3\beta_{j,i}^{k}}{\beta_{max}} \quad (10)$$

where μ is the track-terrain friction coefficient. $F_{zj,i}^{k}$ is the dynamics vertical load, $\sigma_{j,i}^{k}$ the slip ratio and $\beta_{j,i}^{k}$ the slip angle where $k = 1,2$ refers to the front and rear modules, $j = L,R$ to left and right track side and $i = 1,..,N = 4$ to each track-terrain contact point. The dependence upon the longitudinal slip and sideslip angle can be tuned using the two thresholds σ_{max} and β_{max}. In Fig. 4, the track characteristics used for simulations are reported; the threshold values are set to 8° for lateral slip and 0.2 for longitudinal slip.

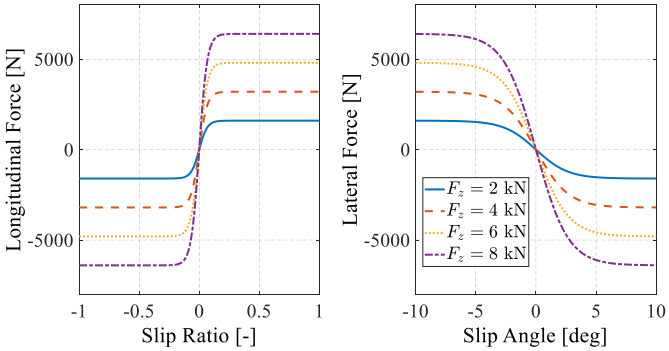

Figure 4. Longitudinal force as a function of longitudinal slip (on the left) and lateral force as a function of slip angle (on the right) used for each contact patch at constant vertical load and track-terrain friction coefficient ($\mu = 0.8$).

Additional coefficients k_{σ} and k_{β}, mapped as functions of slip ratio and slip angle respectively, are introduced into the Eq. (10) to describe the effect of the track combined slip and are implemented by means of look-up tables.

More detailed track-terrain models are available in the literature, able to predict the track motion resistance as well as the tractive effort as functions of soil properties [1]. For the sake of simplicity, a basic model with the lowest possible number of parameters is preferred but maintaining a good level of approximation of the physical phenomenon.

Road Wheels Kinematics

Each road wheel rotational centre has speed that differs from the centre of gravity one when the ATV is turning:

$$\begin{cases} u_{L,i}^{k} = u_{k} - \dot{\psi}_{k}T/2 \\ v_{L,i}^{k} = v_{k} + \dot{\psi}_{k}(d_{i}^{k} - x_{Gk}) \end{cases} \quad \begin{cases} u_{R,i}^{k} = u_{k} + \dot{\psi}_{k}T/2 \\ v_{R,i}^{k} = v_{k} + \dot{\psi}_{k}(d_{i}^{k} - x_{Gk}) \end{cases} \quad (11)$$

where $u_{L,i}^{k}$, $v_{L,i}^{k}$ are longitudinal and lateral speed components of the k_{th} module left side i_{th} road wheel. $u_{R,i}^{k}$, $v_{R,i}^{k}$ are longitudinal and lateral speed components of the k_{th} module right side i_{th} road wheel.

The definition of slip ratios $\sigma_{j,i}^{k}$ and slip angles $\beta_{j,i}^{k}$ are expressed by Equations (12)-(13):

$$\begin{cases} 1 - \dfrac{u_{j,i}^{k}}{V_{j}^{k}} & Traction \\ \dfrac{V_{j}^{k}}{u_{j,i}^{k}} - 1 & Braking \end{cases} \quad (12)$$

where $V_{j}^{k} = \omega_{sj}^{k}R_{s}$ is the pure-rolling speed of j_{th} side track and ω_{sj}^{k} is the j_{th} sprocket angular speed referred to the k_{th} module. The traction condition is identified when $u_{j,i}^{k} \leq V_{j}^{k}$, vice versa for the braking condition.

$$\beta_{j,i}^{k} = \text{atan}\frac{v_{j,i}^{k}}{u_{j,i}^{k}} \quad (13)$$

Depending on the ATV yaw moment equilibrium, each contact patch can laterally slip with concordant or discordant direction with respect to centres of gravity, thus generating yaw moment contributions M_{z}^{k} that can stabilize or destabilize the ATV cornering response.

Vertical Loads

The last contribution required to calculate the forces applied by the i_{th} contact patch, using Eq. (10), is the computation of vertical loads. The normal load acting on the i_{th} contact patch during a cornering manoeuvre is due to a couple of contributions: the static vehicle weight distribution dependent on the vehicle's CG position and the lateral load transfer mainly due to the vehicle's lateral acceleration:

$$F_{zj,i}^{k} = F_{z\,st,i}^{k} + \Delta F_{zj,i}^{k} \quad (14)$$

$F_{z\,st,i}^{k}$ is the static load acting on the i_{th} contact patch when the weight is the only external forces on the k_{th} module (rest position); $\Delta F_{zj,i}^{k}$ represents the lateral load transfer due to lateral acceleration:

$$\Delta F_{zj,i}^{k} = \pm\frac{m_{k}a_{yk}h_{Gk}}{TN} \quad (15)$$

where h_{Gk} is k_{th} center of gravity height with respect to the ground. Sign $+$ applies to the contact patches of the right track, while sign $-$ applies to the ones belonging to the left track, according to the adopted sign convention in Fig. 3. This is calculated assuming that the center of gravity is placed longitudinally in the middle of the contact length and without eccentricity in the transversal direction. The lateral load transfer is equally shared out among all the contact patches of a track, as all the axles are considered to have the same roll stiffness.

Sprocket wheels dynamics

The sprocket wheels angular speed ω_{sj}^{k}, used in Eq. (12), is obtained by integrating the rotational equilibrium equation:

$$I_{s,eq}\dot{\omega}_{sj}^{k} = \frac{C_{M}\eta\tau}{4} - C_{Roll,j}^{k}\frac{R_{s}}{R_{w}} - \sum_{i=1}^{N}F_{xj,i}^{k}\ R_{s} \quad (16)$$

where C_{M} is the engine torque, η is the overall transmission efficiency, τ is the speed ratio between engine shaft and sprocket wheel, R_{s} is the sprocket wheel radius, R_{w} the road wheel radius,

$C^k_{Roll,j}$ is the j_{th} track rolling resistance on the k_{th} module and $I_{s,eq}$ is the equivalent moment of inertia around sprocket wheel axis expressed by:

$$I_{s,eq} = I_s + 4I_w\left(\frac{R_s}{R_w}\right)^2 + \frac{I_M \eta \tau^2}{4} \tag{17}$$

where I_s, I_w, I_M are the sprocket wheel, road wheel and engine shaft moment of inertia respectively.

The track rolling resistance is obtained by summing the rolling resistance applied to each road wheel, finally reported to the sprocket wheel by:

$$C^k_{Roll,j} = \sum_{i=1}^{N} F^k_{zj,i} R_w \left(f_0 + f_2\left(V^k_j\right)^2\right) \tanh\left(\frac{R_s}{R_w}\frac{\omega^k_{sj}}{\omega_{th}}\right) \tag{18}$$

where f_0 and f_2 are rolling resistance coefficients. A hyperbolic tangent function is adopted to smooth the rolling resistance sign change; this transition can be tuned by the threshold ω_{th} which is set to $0.1\frac{rad}{s}$.

Longitudinal Speed Control logic

Since the paper focuses on lateral dynamics analysis, most of results presented in the next section, are obtained at constant longitudinal ATV front module speed. A simple Proportional Integrative (PI) control logic is implemented to track the desired reference longitudinal speed u_{des} during cornering maneuvers. The engine torque C_M in Eq. 16 is then calculated as output of a PI controller:

$$C_M = K_{P,u} e_{u1} + K_{I,u} \int e_{u1}\, dt \tag{19}$$

where $e_{u1} = u_{des} - u_1$ is the ATV front module longitudinal speed error. $K_{P,u}$ and $K_{I,u}$ are the proportional and integral gains of PI logic. The PI gains are tuned in order to have a smooth speed controller, avoiding extremely high dynamic engine torque requests and thus reducing the impact of longitudinal track forces on lateral ones.

Simulation Results

The ATV mathematical model has two input:

- the engine torque C_M, usually requested by the driver by imposing the gas pedal position
- the steering torque C_s, generated by EHPS when a steering wheel angle is set

The engine torque input is obtained through Eq. 19 in order to keep the desired ATV longitudinal speed u_{des} during cornering maneuvers (without generating excessive longitudinal forces).

The steering torque C_s represents the only input of interest in this paper and how it affects ATV kinematics and dynamics behaviors.

Ramp Steering Torque

The maneuver, here called *ramp steering torque*, consists of ramping up the steering torque C_s, meanwhile the ATV speed is kept constant to a desired set value. The ramp steering torque presents a low slope (i.e. 8 Nm/s) in order to smoothly achieve the max ATV lateral acceleration without triggering high frequency dynamics components in the system response. An example of simulation results obtained for $u_{des} = 5\ km/h$ is shown in Fig. 5 and Fig. 6.

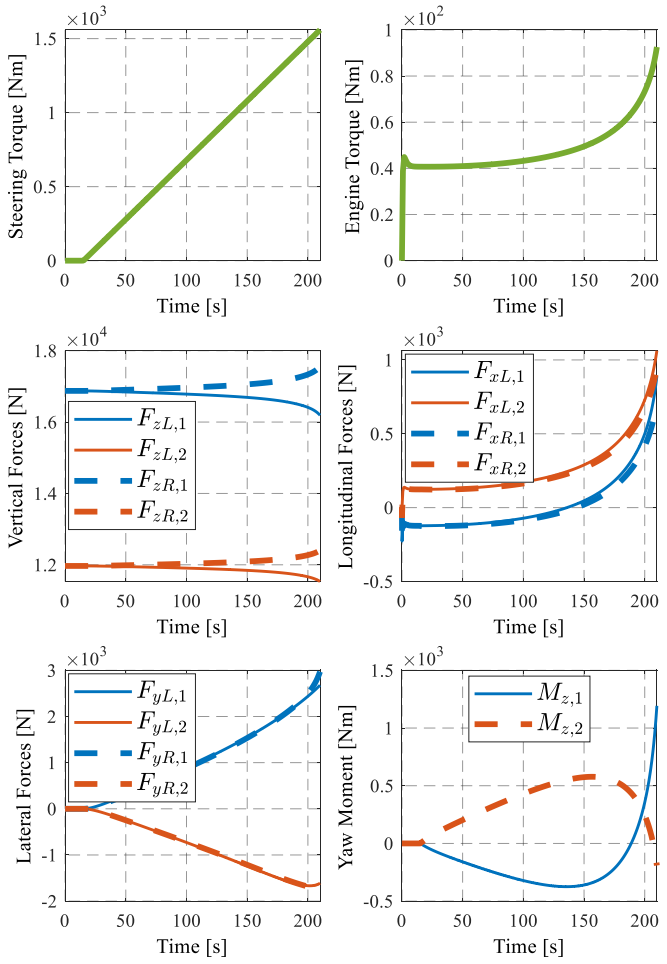

Figure 5. Ramp steering torque at 5 km/h and $\mu = 0.8$: steering torque, engine torque, track-terrain forces and yaw moment vs time.

Fig. 5 shows the steering and engine torques applied to the system with k_{th} module's total left/right longitudinal force $F^k_{xL/R}$, lateral force $F^k_{yL/R}$ and vertical force $F^k_{zL/R}$ together with the yaw moments M^k_z:

$$F^k_{xL/R} = \sum_{i=1}^{N} F^k_{xL/R,i} \quad F^k_{yL/R} = \sum_{i=1}^{N} F^k_{yL/R,i} \quad F^k_{zL/R} = \sum_{i=1}^{N} F^k_{zL/R,i} \tag{20}$$

Longitudinal forces are small enough to avoid any interference with lateral forces and show that the rear module is "pushing" the front one. Yaw moments M^k_z are almost symmetric and presents an opposite sign thus implying that track-terrain forces are decreasing yaw rate (stabilizing yaw moment) for the front module and increasing yaw rate (destabilizing yaw moment) for the rear one.

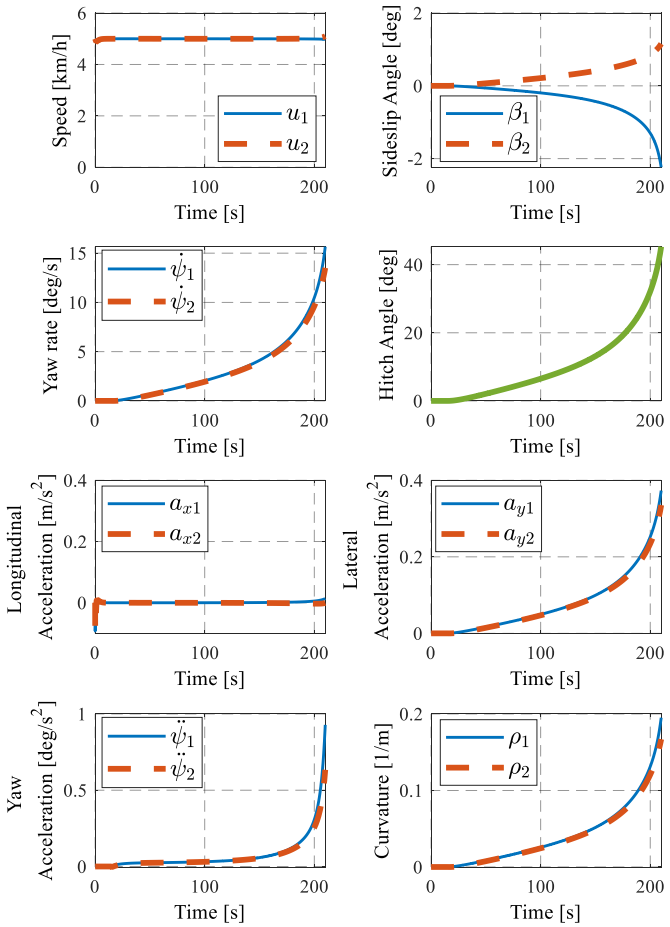

Figure 6. Ramp steering torque at 5 km/h and $\mu = 0.8$: longitudinal speed, sideslip angle, yaw rate, hitch angle, longitudinal acceleration, lateral acceleration, yaw acceleration and curvature for both modules.

Fig. 6 shows ATV speeds and accelerations during the maneuver. Modules curvature ρ_1 and ρ_2 are calculated as:

$$\rho_k = \frac{a_{yk}u_k - a_{xk}v_k}{V_k^3} \tag{21}$$

Curvatures are overlapped over time thus indicating that the two modules are turning with the same radius.

A linear dependence between all quantities and steering torque is observed in the first part of the maneuver, but it is evident that yaw accelerations change rapidly in the last part. This represents a critical behavior also highlighted by high yaw rate and sideslip angle values at the end of the maneuver.

The ramp steering torque is adopted to smoothly increased the ATV lateral acceleration up to the maximum value achievable. For this reason, sideslip angle, curvature and the hitch angle are plotted as function of the front module lateral accelerations in Fig. 7.

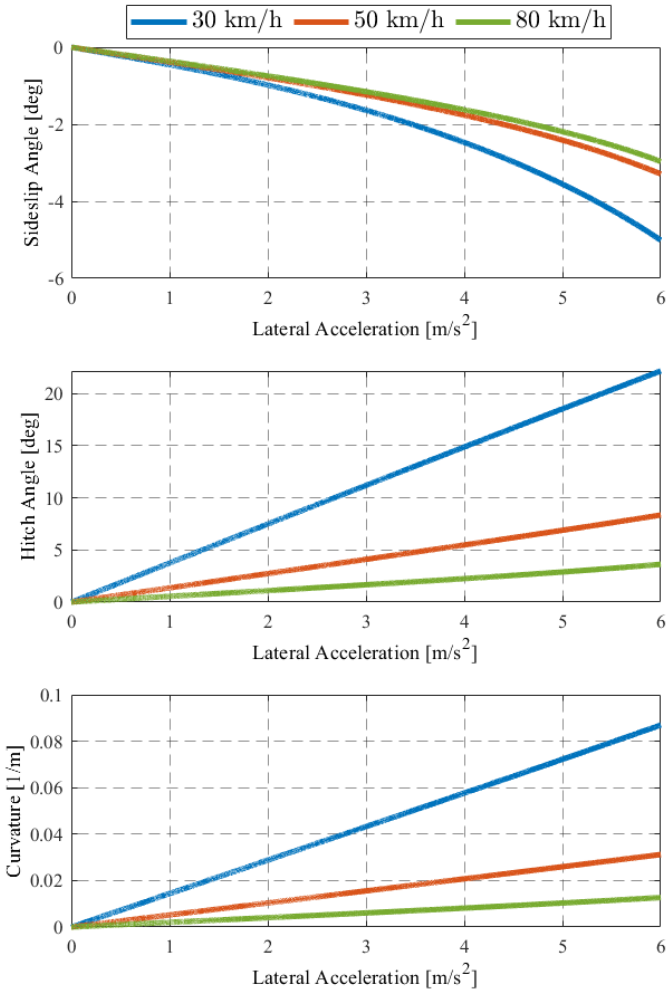

Figure 7. Ramp steering torque at 30-50-80 km/h and $\mu = 0.8$: modules' sideslip angle, hitch angle and curvature of the front module vs its center of gravity lateral acceleration.

The hitch angle, together with the curvature, shows a linear relation with respect to the lateral acceleration thus representing a good parameter for controlling the ATV lateral behavior. It is interesting how the steering torque is related to lateral acceleration, as shown in Fig.8.

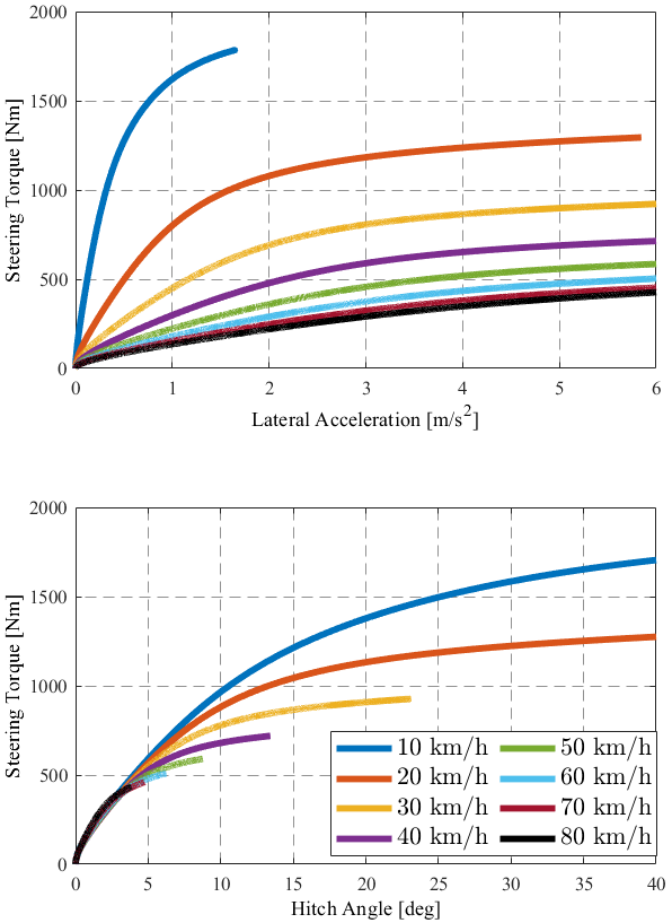

Figure 8. Ramp steering torque at different speeds and $\mu = 0.8$: steering torque versus first module's lateral accelerations (up) and steering torque versus hitch angle (down).

In the up-side part of Fig. 8, each curve presents a linear region that tends to saturate for higher lateral accelerations. In the linear region, a greater steering torque must be applied in order achieve the same lateral acceleration at lower speeds, thus also implying higher lateral track-terrain lateral forces and corresponding sideslip angles. More interesting is the saturation region, where any further increase of steering torque does not provoke a proportional increase of lateral acceleration. A similar result is shown in the down-side of Fig. 8 where the steering torque is plotted versus the hitch angle: a small increase of steering torque would cause a great increase of hitch angle, thus leading to a destabilizing and critical situation.

This phenomenon is clearer and more evident by executing two *step steering torque* maneuvers: one with a steering torque in the linear region and the other one in the saturation region. In both cases, the steering torque step is applied at time step $t = 0$.

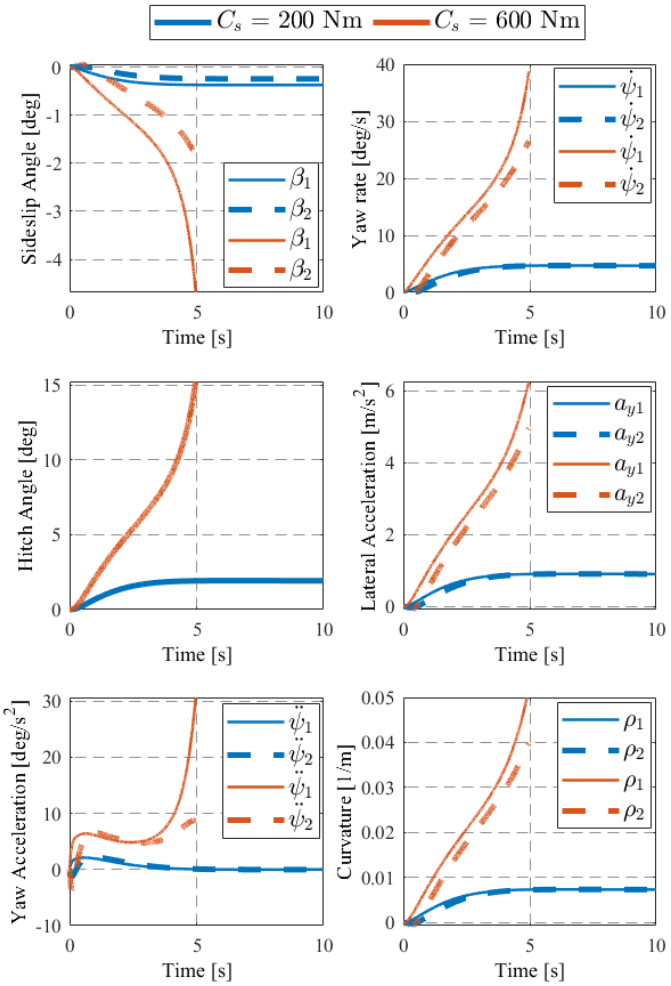

Figure 9. Step steering torque at 40 km/h and $\mu = 0.8$: sideslip angle, yaw rate, hitch angle, lateral acceleration, yaw acceleration and curvature for both modules at constant steering torque $C_s = 200\ Nm$ (red lines) and $C_s = 600\ Nm$ (blue lines).

Fig. 9 clearly shows that the ATV, with open-loop steering torque as input, is not a Bounded-Input Bounded-Output (BIBO) system: output quantities (i.e. curvature, sideslip angle and yaw rate) are not bounded for every input (steering torque) that is bounded.

These results imply that the steering torque must be properly controlled in order to avoid critical situations as in Fig.9. The solution proposed by the authors is to include a feedback control on a kinematic quantity. The hitch angle represents a good choice since it refers to the whole ATV curvature.

Ramp Hitch Angle

A close-loop controller on the hitch angle is suitable for obtaining a BIBO stable system.

A proportional steering torque control is introduced for tracking a desired hitch angle α_{des} (and so a desired curvature):

$$C_s = K_{P,\alpha} e_\alpha \tag{22}$$

where $e_{\alpha} = \alpha_{des} - \alpha$ is the hitch angle error with respect the desired value and $K_{P,\alpha}$ is a proportional gain.

In order to understand the kinematic behavior of the ATV, a *ramp hitch angle* maneuver is executed at low speed. It consists in smoothly ramping up the desired hitch angle to the maximum physical limit of 40 deg. The desired hitch angle slope is selected low on purpose to impose a quasi-static behavior thus also avoiding any contribution due to the damping effect $c_O\dot{\alpha}$.

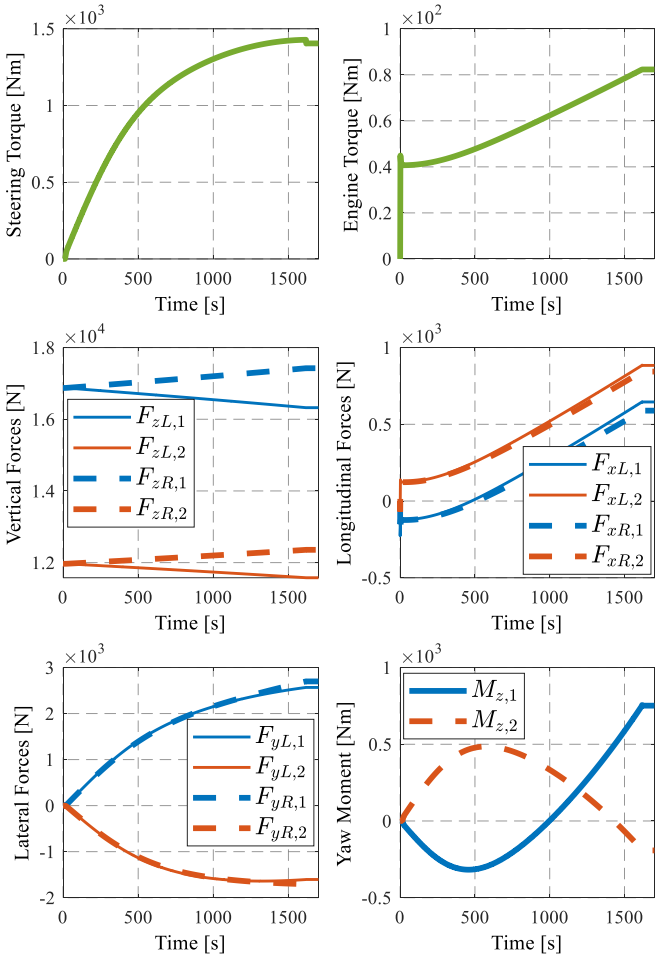

Figure 10. Ramp hitch angle at 5 km/h and $\mu = 0.8$: steering torque, engine torque, track-terrain forces and yaw moment vs time.

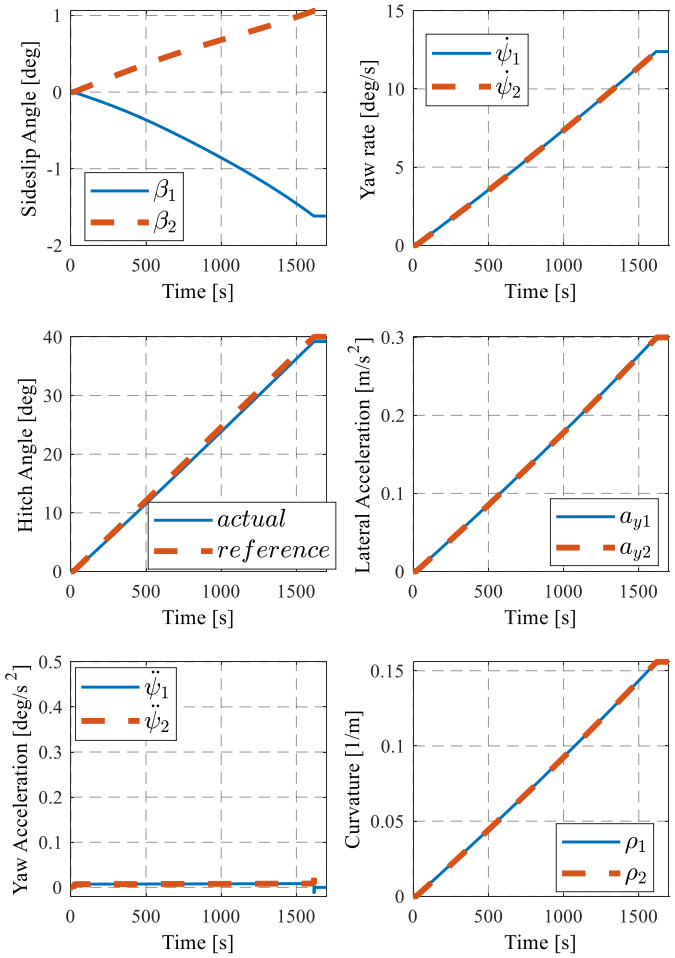

Figure 11. Ramp hitch angle at 5 km/h and $\mu = 0.8$: sideslip angle, yaw rate, hitch angle, lateral acceleration, yaw acceleration and curvature for both modules.

Fig. 10 shows that the steering torque must be smoothly saturated if a linear and stable variation of hitch angle (and thus a linear ATV curvature) is desired. This is mainly due to the yaw moments M_z^k generated by track-terrain forces on the k_{th} module: a sign inversion on both modules also appears here but, differently from ramp steering torque results in Fig. 5, the application of steering torque is reduced when the curvature increases. Fig. 11 proves that the maneuver is stable, since the yaw acceleration is not diverging as in the ramp steering torque maneuver. The hitch angle control is thus able to provide a stable regulation of modules curvature, yaw rate and lateral accelerations.

Due to the low speed and lateral acceleration reached during this maneuver, it can be considered representative of the ATV kinematic behavior. What is different from the theory of a conventional passenger car behaviors is that, all track-terrain contact patches present a non-null slip angle even in kinematic conditions: the generation of slip angles, and thus of lateral forces, is fundamental for turning the ATV even at low speed conditions.

It is of interest to calculate the relation between kinematic hitch angle and sideslip angles versus the curvature thus introducing the following gains e_{α}^k and e_{β}^k:

$$e_\alpha^k = \frac{\alpha^{kin}}{\rho_k} \quad e_\beta^k = \frac{\beta_k^{kin}}{\rho_k} \tag{23}$$

where α^{kin} and β_k^{kin} are obtained from the ramp hitch angle maneuver at $u_{des} = 5$ km/h. These gains are almost constant as function of curvatures ρ_k, as shown in Fig.12.

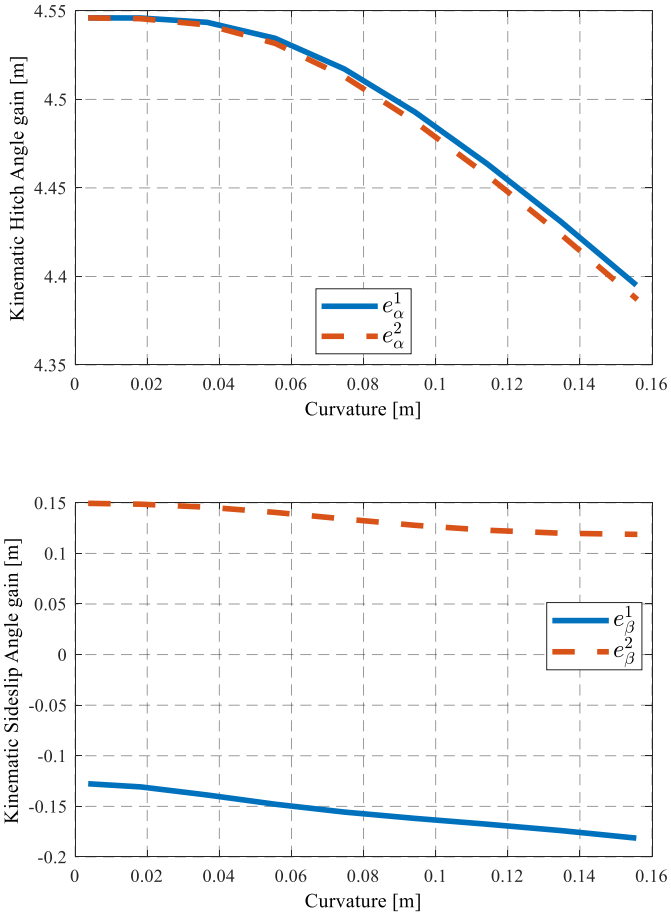

Figure 12. Hitch angle (up) and sideslip angle (down) kinematic characteristics.

It is remarkable to notice that α^{kin} and β_k^{kin} share the same meaning of wheeled vehicles kinematic steering angle and sideslip angle: the gains e_α^k and e_β^k could represent the equivalent wheelbase and rear semi wheelbase respectively.

By storing α^{kin} and β_k^{kin} in a Look-Up table as function of ρ_k, it is possible to calculate the dynamic hitch angle and dynamic sideslip angles for higher lateral acceleration conditions (i.e. non kinematic conditions):

$$\alpha^{dyn} = \alpha - \alpha^{kin} \quad \beta_k^{dyn} = \beta - \beta_k^{kin} \tag{24}$$

The definition of α^{dyn} and β_k^{dyn} are important to understand how the hitch angle and sideslip angles deviates from the kinematic behavior during high lateral acceleration condition.

By executing the ramp hitch angle maneuver for different speeds, the handling characteristics are extrapolated in Fig. 13.

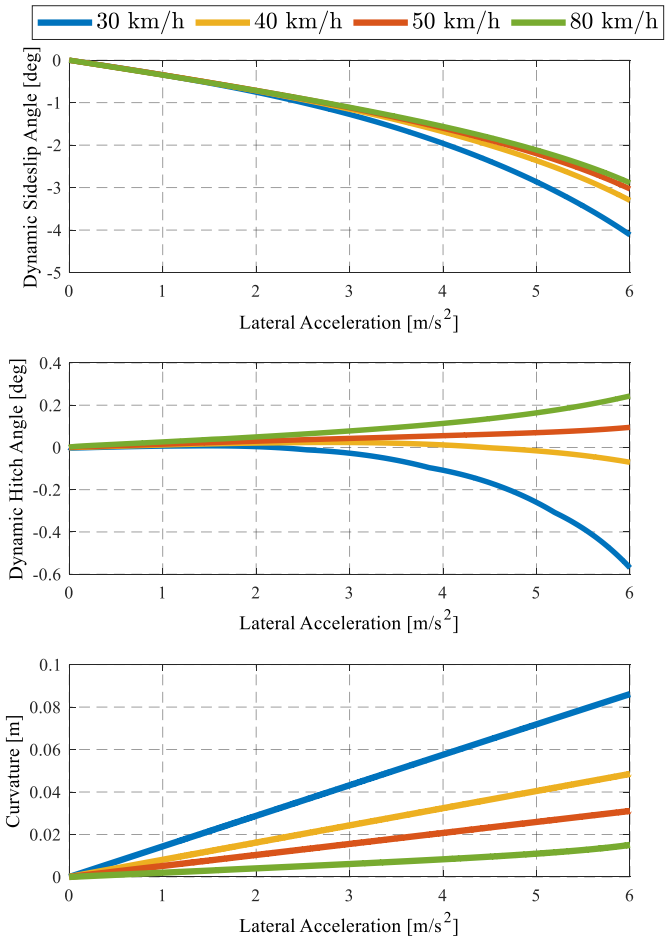

Figure 13 Ramp hitch angle at 30-40-50-80 km/h and $\mu = 0.8$: modules' dynamic sideslip angle, dynamics hitch angle and curvature of the front module vs its center of gravity lateral acceleration.

The dynamic hitch angle is very small which means that the hitch angle required to follow a specific curvature at higher lateral acceleration is very close to the correspondent kinematic value. The dynamic hitch angle shows also a sign change for speeds lower than 40 km/h, which means that at low speed a small counteraction of the hitch angle is required to follow the same trajectory.

The dynamic sideslip angle is speed-independent only for speeds greater than 40 km/h: at lower speed, higher lateral slips is required to turn the ATV.

The curvature shows a linear correlation to the lateral acceleration; only for high speed (80 km/h), the trend tends to smoothly approach towards an asymptotic axis.

The effect of longitudinal speed on steering torque characteristics is described by Fig. 14.

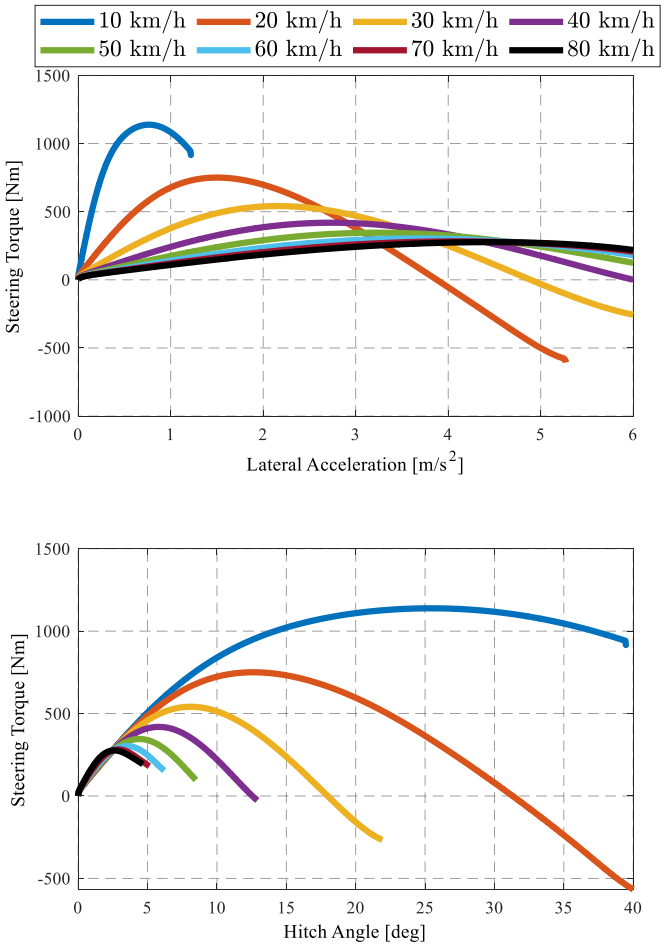

Figure 14. Ramp hitch angle at different speeds and $\mu = 0.8$: steering torque versus first module's lateral accelerations (up) and steering torque versus hitch angle (down).

It is evident the difference with respect to Fig. 8: for each speed, the steering torque must be reduced when lateral acceleration exceeds a speed-related threshold. For some speeds, the sign of the steering torque could even change at high lateral accelerations: the M_z^k becomes greater than the moment generated by inertial forces due to a_y, so a counteracting steering torque is required to stabilize the ATV.

Conclusions

The non-linear mathematical model, focus of this paper, is implemented to understand the kinematic and dynamic behavior of a bi-modular ATV.

The simulation results achieved through specific steady-state maneuvers led to the following conclusions:

- The application of an open-loop steering torque is not enough to manage the trajectory of the ATV without any feedback from kinematics quantities: for high trajectory curvatures, the application of a steering torque may compromise vehicle stability.
- The hitch angle represents a good choice for introducing a closed-loop control for steering torque regulation.
- In low lateral acceleration conditions (low speed ramp maneuver), a relation between hitch angle and sideslip angles with respect to curvature is obtained: the ATV turning requires always a slip condition between the track and the terrain even at low speeds.
- In high lateral acceleration conditions, the hitch angle required to track the same curvature is very close to the kinematic hitch angle.
- In high lateral acceleration conditions and lower speed, a small reduction of hitch angle (counteraction) is needed to track the same curvature with respect the kinematic condition.

References

1. Wong, Jo Yung. Terramechanics and off-road vehicle engineering: terrain behaviour, off-road vehicle performance and design. Butterworth-heinemann, 2009.
2. Muro, Tatsuro, and Jonathan O'Brien. Terramechanics: land locomotion mechanics. CRC Press, 2004.
3. Bekker, Mieczyslaw Gregory. "Theory of land locomotion." (1956).
4. Maclaurin, Bruce. "A skid steering model with track pad flexibility." Journal of Terramechanics 44.1 (2007): 95-110.
5. Maclaurin, B. "Corrigendum to "A skid steering model with track pad flexibility [J Terramech 2007; 44 (1): 95–110]"." Journal of Terramechanics 2.44 (2007): 217-218.
6. Guo, Tianyou, and Huei Peng. "A simplified skid-steering model for torque and power analysis of tracked small unmanned ground vehicles." 2013 American Control Conference. IEEE, 2013.
7. Maclaurin, Bruce. "Comparing the steering performances of skid-and Ackermann-steered vehicles." Proceedings of the Institution of Mechanical Engineers, Part D: Journal of Automobile Engineering 222.5 (2008): 739-756.
8. Hohl, Guenter H. "Military terrain vehicles." Journal of Terramechanics 44.1 (2007): 23-34.
9. Maclaurin, E. B., and D. A. Crolla. "Wheel spin control for on/off road vehicles." Traction Control and Anti Wheel Spin Systems for Road Vehicles, International Conference, London, United Kingdom. 1988.
10. Horton, D. N. L., and D. A. Crolla. "Theoretical analysis of the steering behaviour of articulated frame steer vehicles." Vehicle System Dynamics 15.4 (1986): 211-234.
11. Pazooki, Alireza, Subhash Rakheja, and Dongpu Cao. "Kineto-dynamic directional response analysis of an articulated frame steer vehicle." International Journal of Vehicle Design 65.1 (2014): 1-30.
12. Gao, Yu, et al. "Oscillatory Yaw Motion Control for Hydraulic Power Steering Articulated Vehicles Considering the Influence of Varying Bulk Modulus." IEEE Transactions on Control Systems Technology 27.3 (2018): 1284-1292.
13. He, Yuping, et al. "Dynamic modelling and stability analysis of articulated frame steer vehicles." International Journal of Heavy Vehicle Systems 12.1 (2005): 28-59.
14. Liu, Yugang, and Guangjun Liu. "Modeling of tracked mobile manipulators with consideration of track–terrain and vehicle–manipulator interactions." Robotics and Autonomous Systems 57.11 (2009): 1065-1074.
15. Galvagno, Enrico, Enzo Rondinelli, and Mauro Velardocchia. "Electro-mechanical transmission modelling for series-hybrid tracked tanks." International Journal of Heavy Vehicle Systems 19.3 (2012): 256-280.

16. Venturini, S., Bonisoli E. " Design of a spherical pendulum didactic test rig " International Journal of Mechanics and Control. 19.1 (2018):69-76.

Contact Information

Antonio Tota

(+39) 3356294176

antonio.tota@polito.it